SCIENCE CHINA
Information Sciences

• Supplementary File •

On covert transmission of distributed antenna systems against heterogeneous adversaries

Weiyu CHEN[1], Haiyang DING[2], Shilian WANG[1*], Junshan LUO[1,3] & Fengkui GONG[4]

[1]*College of Electronic Science and Technology, National University of Defense Technology, Changsha 410073, China*
[2]*Engineering University of Information Support Force, Wuhan 430019, China*
[3]*The Sixty-Third Research Institute, National University of Defense Technology, Nanjing 210007, China*
[4]*State Key Laboratory of Integrated Service Networks, Xidian University, Xi'an 710071, China*

Appendix A Proof of Lemma 1

According to equation (11), equation $\xi\left(P_b,t\right)\equiv 0$ holds when $|h|^2>P_{\max}|g|^2$ and $t\in\left[P_{\max}|g|^2+\sigma_w^2,|h|^2+\sigma_w^2\right]$. Now we turn to the case when $|h|^2\leqslant P_{\max}|g|^2$. We firstly expand $E\left\{\xi\left(P_b,t\right)\right\}$ as

$$E\left\{\xi\left(P_b,t\right)\right\}=\Pr\left\{P_b>\frac{t-\sigma_w^2}{|g|^2}\right\}+\Pr\left\{P_b<\frac{t-|h|^2-\sigma_w^2}{|g|^2}\right\}. \tag{A1}$$

As P_b follows $\mathrm{U}\left(0,P_{\max}\right)$, we have

$$\Pr\left\{P_b>\frac{t-\sigma_w^2}{|g|^2}\right\}=\begin{cases}0, & \frac{t-\sigma_w^2}{|g|^2}>P_{\max},\\ \frac{P_{\max}-\frac{t-\sigma_w^2}{|g|^2}}{P_{\max}}, & 0\leqslant\frac{t-\sigma_w^2}{|g|^2}\leqslant P_{\max},\\ 1, & t<\sigma_w^2,\end{cases} \tag{A2}$$

$$\Pr\left\{P_b<\frac{t-|h|^2-\sigma_w^2}{|g|^2}\right\}=\begin{cases}1, & \frac{t-|h|^2-\sigma_w^2}{|g|^2}>P_{\max},\\ \frac{t-|h|^2-\sigma_w^2}{P_{\max}|g|^2}, & 0\leqslant\frac{t-|h|^2-\sigma_w^2}{|g|^2}\leqslant P_{\max},\\ 0, & t<|h|^2+\sigma_w^2.\end{cases} \tag{A3}$$

Next, note that equation $\xi\left(P_b,t\right)\equiv 1$ holds when $t\geqslant|h|^2+P_{\max}|g|^2+\sigma_w^2$. When $|h|^2+P_{\max}|g|^2+\sigma_w^2>t>P_{\max}|g|^2+\sigma_w^2$, we have $\Pr\left\{P_b>\frac{t-\sigma_w^2}{|g|^2}\right\}\equiv 0$, whereas $\Pr\left\{P_b<\frac{t-|h|^2-\sigma_w^2}{|g|^2}\right\}$ is monotonically increasing with t and meanwhile is smaller than 1. As a result, we can conclude that $t^*\leqslant P_{\max}|g|^2+\sigma_w^2$. Similarly, note that equation $\xi\left(P_b,t\right)\equiv 1$ holds when $t\leqslant\sigma_w^2$. When $\sigma_w^2<t<|h|^2+\sigma_w^2$, we have $\Pr\left\{P_b<\frac{t-|h|^2-\sigma_w^2}{|g|^2}\right\}\equiv 0$, whereas $\Pr\left\{P_b>\frac{t-\sigma_w^2}{|g|^2}\right\}$ is monotonically decreasing with t and meanwhile is smaller than 1. As a result, we have $t^*\geqslant|h|^2+\sigma_w^2$. Finally, when $|h|^2+\sigma_w^2\leqslant t\leqslant P_{\max}|g|^2+\sigma_w^2$, it follows from (A2) and (A3) that

$$E\left\{\xi\left(P_b,t\right)\right\}=\frac{P_{\max}-\frac{t-\sigma_w^2}{|g|^2}}{P_{\max}}+\frac{t-|h|^2-\sigma_w^2}{P_{\max}|g|^2}\equiv 1-\frac{|h|^2}{P_{\max}|g|^2}, \tag{A4}$$

which completes the proof.

Appendix B Proof of Proposition 1

For the j-th ground Willie, it follows from (4) that $h=\sum_{i=1}^{N_a}\sqrt{\frac{P_i}{d_{g,i,j}^{\alpha(0)}}}h_{g,i,j}e^{\iota\varphi_i}$ and $g=\frac{1}{\sqrt{d_{g,b,j}^{\alpha\left(\Theta_{g,b,j}\right)}}}h_{g,b,j}$. Herein, $|h|^2$ follows exponential distribution with mean $\sum_{i=1}^{N_a}\frac{P_i}{d_{g,i,j}^{\alpha(0)}}$. The probability density function (PDF) of $|g|^2$ is $f_{|g|^2}\left(y\right)=$

* Corresponding author (email: wangsl@nudt.edu.cn)

$\mathcal{K}\exp\left(-K\left(\Theta_{g,b,j}\right)-\mathcal{K}y\right)I_0\left(2\sqrt{K\left(\Theta_{g,b,j}\right)\mathcal{K}y}\right)$, where $\mathcal{K}\triangleq d_{g,b,j}^{\alpha(\Theta_{g,b,j})}\left(K\left(\Theta_{g,b,j}\right)+1\right)$. Thus, we have

$$\begin{aligned}\Pr\left\{|h|^2\leqslant\epsilon P_{\max}|g|^2\right\}=&\int_0^\infty\left[1-\exp\left(-\frac{\epsilon P_{\max}y}{\sum_{i=1}^{N_a}\frac{P_i}{d_{g,i,j}^{\alpha(0)}}}\right)\right]f_{|g|^2}(y)\,dy\\=&1-\mathcal{K}e^{-K(\Theta_{g,b,j})}\int_0^\infty\exp\left(-\left[\frac{\epsilon P_{\max}}{\sum_{i=1}^{N_a}\frac{P_i}{d_{g,i,j}^{\alpha(0)}}}+\mathcal{K}\right]y\right)I_0\left(2\sqrt{K\left(\Theta_{g,b,j}\right)\mathcal{K}y}\right)dy.\end{aligned}\tag{B1}$$

To proceed, we define $\varrho\triangleq\frac{\epsilon P_{\max}}{\sum_{i=1}^{N_a}\frac{P_i}{d_{g,i,j}^{\alpha(0)}}}+\mathcal{K}$ and $\beta\triangleq K\left(\Theta_{g,b,j}\right)\mathcal{K}$. By applying [1, Eq. (6.614.3)], we have

$$\begin{aligned}\Pr\left\{|h|^2\leqslant\epsilon P_{\max}|g|^2\right\}&=1-\mathcal{K}e^{-K(\Theta_{g,b,j})}\frac{e^{\frac{1}{2}\frac{\beta}{\varrho}}}{\sqrt{\varrho\beta}}M_{-\frac{1}{2},0}\left(\frac{\beta}{\varrho}\right)\\&=1-\frac{\beta}{K\left(\Theta_{g,b,j}\right)}e^{-K(\Theta_{g,b,j})}\frac{e^{\frac{1}{2}\frac{\beta}{\varrho}}}{\sqrt{\varrho\beta}}M_{-\frac{1}{2},0}\left(\frac{\beta}{\varrho}\right)\\&=1-\frac{\sqrt{\frac{\beta}{\varrho}}e^{\frac{1}{2}\frac{\beta}{\varrho}}M_{-\frac{1}{2},0}\left(\frac{\beta}{\varrho}\right)}{K\left(\Theta_{g,b,j}\right)e^{K(\Theta_{g,b,j})}},\end{aligned}\tag{B2}$$

where $M_{\cdot,\cdot}(\cdot)$ is the Whittaker function [1, Eq. (9.220.2)]. Furthermore, by applying [1, Eq. (9.215.1)], we can arrive at equation (14), which completes the proof.

Appendix C Proof of Proposition 2

For the j-th near UAV Willie, it follows from (5) that $h=\sum_{i=1}^{N_a}\sqrt{\frac{P_i}{d_{c,i,j}^{\alpha(\Theta_{c,i,j})}}}h_{c,i,j}e^{\iota\varphi_i}$ and $g=\sqrt{\frac{1}{d_{c,b,j}^2}}e^{\iota\psi_{c,b,j}}$. To proceed, we expand h as

$$h=\sum_{i=1}^{N_a}\left[\sqrt{\frac{P_i}{d_{c,i,j}^{\alpha(\Theta_{c,i,j})}}}\sqrt{\frac{K\left(\Theta_{c,i,j}\right)}{K\left(\Theta_{c,i,j}\right)+1}}e^{\iota\left(\psi_{c,i,j}+\varphi_i\right)}\right]+\sum_{i=1}^{N_a}\left[\sqrt{\frac{P_i}{d_{c,i,j}^{\alpha(\Theta_{c,i,j})}}}\sqrt{\frac{1}{K\left(\Theta_{c,i,j}\right)+1}}\hat{h}_{c,i,j}e^{\iota\varphi_i}\right].\tag{C1}$$

Note that the first term of the RHS of (C1) is the sum of N_a variables with different modulus $V_i\triangleq\sqrt{\frac{P_i}{d_{c,i,j}^{\alpha(\Theta_{c,i,j})}}}\sqrt{\frac{K(\Theta_{c,i,j})}{K(\Theta_{c,i,j})+1}}$ $(i=1,2,\ldots,N_a)$ and random phases independently following $\mathrm{U}\left(0,2\pi\right)$. The second term is the sum of N_a independent complex Gaussian variables. As a result, the second term follows $\mathcal{CN}\left(0,2\sigma^2\right)$, where $2\sigma^2\triangleq\sum_{i=1}^{N_a}\left[\frac{P_i}{d_{c,i,j}^{\alpha(\Theta_{c,i,j})}(K(\Theta_{c,i,j})+1)}\right]$. In addition, note that the second term is independent of the first term because $\hat{h}_{c,i,j}$ is independent of $\psi_{c,i,j}$. Combining the foregoing observations, it is noted that h is equivalently multiple waves with diffuse power (MWDP) [2,3]. The PDF of $|h|$ is [2]

$$f_{|h|}(x)=x\int_0^\infty J_0\left(vx\right)\exp\left(-\frac{v^2\sigma^2}{2}\right)\left[\prod_{i=1}^{N_a}J_0\left(V_iv\right)\right]vdv,x\geqslant0.\tag{C2}$$

After variable substitution, one can obtain equation (16), which does not have a closed-form expression. For such, it is noted that the PDF of $|h|$ can be well approximated by [3]

$$f_{|h|}(x)\approx\frac{2x}{\sum_{i=1}^{N_a}V_i^2+2\sigma^2}\exp\left(-\frac{x^2}{\sum_{i=1}^{N_a}V_i^2+2\sigma^2}\right),x\geqslant0,\tag{C3}$$

based on which one can arrive at equation (17).

Appendix D Proof of Proposition 3

For the j-th far UAV Willie, it follows from (6) that $h=\frac{\sqrt{W_f}}{\sqrt{d_{f,j}^{\alpha(\Theta_{f,j})}}}\boldsymbol{h}_{f,j}^T\boldsymbol{w}$ and $g=\sqrt{\frac{w_f}{d_{f,b,j}^2}}e^{\iota\psi_{f,b,j}}$. We expand $\boldsymbol{h}_{f,j}^T\boldsymbol{w}$ as

$$\boldsymbol{h}_{f,j}^T\boldsymbol{w}=\sqrt{\frac{K\left(\Theta_{f,j}\right)}{K\left(\Theta_{f,j}\right)+1}}e^{\iota\psi_{f,j}}\bar{\boldsymbol{h}}_{f,j}^T\boldsymbol{w}+\sqrt{\frac{1}{K\left(\Theta_{f,j}\right)+1}}\hat{\boldsymbol{h}}_{f,j}^T\boldsymbol{w},\tag{D1}$$

which follows $\mathcal{CN}\left(\sqrt{\frac{K(\Theta_{f,j})}{K(\Theta_{f,j})+1}}e^{\iota\psi_{f,j}}\bar{\boldsymbol{h}}_{f,j}^T\boldsymbol{w}, \frac{||\boldsymbol{w}||^2}{K(\Theta_{f,j})+1}\right)$. As a result, the real part of $\boldsymbol{h}_{f,j}^T\boldsymbol{w}$ can be expressed as $R \sim \mathcal{N}\left(\text{real}\left(\sqrt{\frac{K(\Theta_{f,j})}{K(\Theta_{f,j})+1}}e^{\iota\psi_{f,j}}\bar{\boldsymbol{h}}_{f,j}^T\boldsymbol{w}\right), \frac{1}{2}\frac{||\boldsymbol{w}||^2}{K(\Theta_{f,j})+1}\right)$, which is independent of the imaginary part of $\boldsymbol{h}_{f,j}^T\boldsymbol{w}$, given by $I \sim \mathcal{N}\left(\text{imag}\left(\sqrt{\frac{K(\Theta_{f,j})}{K(\Theta_{f,j})+1}}e^{\iota\psi_{f,j}}\bar{\boldsymbol{h}}_{f,j}^T\boldsymbol{w}\right), \frac{1}{2}\frac{||\boldsymbol{w}||^2}{K(\Theta_{f,j})+1}\right)$. Thus, we have

$$\left|\boldsymbol{h}_{f,j}^T\boldsymbol{w}\right|^2 = R^2 + I^2 = \left(\frac{1}{2}\frac{||\boldsymbol{w}||^2}{K\left(\Theta_{f,j}\right)+1}\right)\left(R'^2 + I'^2\right) \triangleq \left(\frac{1}{2}\frac{||\boldsymbol{w}||^2}{K\left(\Theta_{f,j}\right)+1}\right)\Omega, \tag{D2}$$

where random variables R' and I' follow normal distributions $\mathcal{N}\left(\text{real}\left(\sqrt{\frac{K(\Theta_{f,j})}{K(\Theta_{f,j})+1}}e^{\iota\psi_{f,j}}\bar{\boldsymbol{h}}_{f,j}^T\boldsymbol{w}\right)/\sqrt{\frac{1}{2}\frac{||\boldsymbol{w}||^2}{K(\Theta_{f,j})+1}}, 1\right)$ and $\mathcal{N}\left(\text{imag}\left(\sqrt{\frac{K(\Theta_{f,j})}{K(\Theta_{f,j})+1}}e^{\iota\psi_{f,j}}\bar{\boldsymbol{h}}_{f,j}^T\boldsymbol{w}\right)/\sqrt{\frac{1}{2}\frac{||\boldsymbol{w}||^2}{K(\Theta_{f,j})+1}}, 1\right)$, respectively. As a result, $\Omega \triangleq R'^2 + I'^2$ follows the noncentral Chi-Squared distribution [4] with 2 degrees of freedom and noncentrality parameter

$$\begin{aligned}\mathcal{L} =& \left(\text{real}\left(\sqrt{\frac{K\left(\Theta_{f,j}\right)}{K\left(\Theta_{f,j}\right)+1}}e^{\iota\psi_{f,j}}\bar{\boldsymbol{h}}_{f,j}^T\boldsymbol{w}\right)/\sqrt{\frac{1}{2}\frac{||\boldsymbol{w}||^2}{K\left(\Theta_{f,j}\right)+1}}\right)^2 \\ &+ \left(\text{imag}\left(\sqrt{\frac{K\left(\Theta_{f,j}\right)}{K\left(\Theta_{f,j}\right)+1}}e^{\iota\psi_{f,j}}\bar{\boldsymbol{h}}_{f,j}^T\boldsymbol{w}\right)/\sqrt{\frac{1}{2}\frac{||\boldsymbol{w}||^2}{K\left(\Theta_{f,j}\right)+1}}\right)^2 \\ =& \frac{\frac{K(\Theta_{f,j})}{K(\Theta_{f,j})+1}\left|\bar{\boldsymbol{h}}_{f,j}^T\boldsymbol{w}\right|^2}{\frac{1}{2}\frac{||\boldsymbol{w}||^2}{K(\Theta_{f,j})+1}} = 2K\left(\Theta_{f,j}\right)\left|\bar{\boldsymbol{h}}_{f,j}^T\frac{\boldsymbol{w}}{||\boldsymbol{w}||}\right|^2.\end{aligned} \tag{D3}$$

Thus, the cumulative distribution function of Ω is $F_\Omega(x) = 1 - Q_1\left(\sqrt{2K\left(\Theta_{f,j}\right)\left|\bar{\boldsymbol{h}}_{f,j}^T\frac{\boldsymbol{w}}{||\boldsymbol{w}||}\right|^2}, \sqrt{x}\right)$. Finally, we have

$$\Pr\left\{|h|^2 \leqslant \epsilon P_{\max}|g|^2\right\} = \Pr\left\{\frac{W_f}{d_{f,j}^{\alpha(\Theta_{f,j})}}\left(\frac{1}{2}\frac{||\boldsymbol{w}||^2}{K\left(\Theta_{f,j}\right)+1}\right)\Omega \leqslant \epsilon P_{\max}\frac{w_f}{d_{f,b,j}^2}\right\}, \tag{D4}$$

which completes the proof of proposition 3.

Appendix E Locations of the transmit nodes in the simulations

The simulation setup of the coordinates of the transmit nodes is given in Table E1. The results under the case with N_a transmit nodes are based on Node 1, Node 2, ..., and Node N_a.

Table E1 Locations of the transmit nodes in the simulations

Node Num	x coordinate (meter)	y coordinate (meter)
Node 1	-4.52012080336973	1.00682306810280
Node 2	-2.72532990022955	-5.53023030751947
Node 3	0.938931678443398	-3.04831635767469
Node 4	-7.82907084873399	2.68003764645483
Node 5	-5.29743090456251	1.40398390474095
Node 6	8.28021549521095	-0.0193665745900695
Node 7	-3.05738280225871	-9.99522970648069
Node 8	2.40515134425744	-5.49443949752547
Node 9	1.60414267850222	6.95469521781822
Node 10	-7.25294143966018	-1.74065150381521
Node 11	6.88120538326776	3.90852965148370
Node 12	8.16049671186168	-0.414551946322451

As the specific distribution of the transmit nodes influences the numerical results, another set of randomly generated coordinates of the transmit nodes is presented in Table E2, and the performance under distribution 1 (i.e., distribution in Table E1) and that under distribution 2 (i.e., distribution in Table E2) are compared in Figure E1. As can be seen from the figure, the fundamental trend remains as the same for these two distributions.

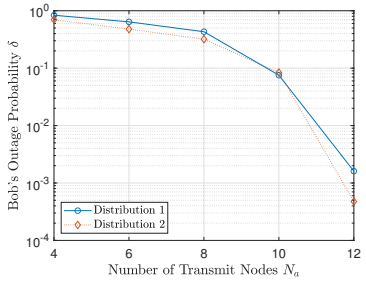

Figure E1 The performance of the proposed algorithm under different transmit node distributions.

Table E2 Locations of the transmit nodes used as distribution 2 in Figure E1

Node Num	x coordinate (meter)	y coordinate (meter)
Node 1	7.96751108561283	0.196745599069519
Node 2	8.98069282968978	5.64214781963892
Node 3	-0.780704578519259	-8.98564924998929
Node 4	-2.79462867033002	3.40904508410317
Node 5	-1.52312184560801	7.57018902072198
Node 6	-8.76152908994881	2.24993420139768
Node 7	-1.52146885061034	7.09722923675890
Node 8	-2.12989594203813	-3.28937266885477
Node 9	-4.83810048248258	1.16240129148536
Node 10	7.30677946567852	6.55919374105897
Node 11	-5.89889458771438	7.89990603911156
Node 12	4.38190656593911	6.89541707449658

Appendix F Simulations of the covert probability

To validate the analytical results and to confirm that the proposed algorithm does satisfy the covert constraints, the covert probabilities at Willies are simulated. The parameters setup is the same as that in Section 5 of the paper. The only difference is that herein the number and the positions of ground Willies should be specified. Without loss of generality, two ground Willies are considered. Their positions are set as $(32, 32, 0)$ and $(-32, -32, 0)$ in meter, respectively. In the simulations, the solution obtained by the proposed algorithm under a specific realization of Bob's channel is used. Based on this solution, 10^6 random realizations of Willies' channels are conducted to simulate the covert probabilities. The results are shown in Table F1. As can be observed from the table, the simulation results match well with the analytical results. The obtained bound and approximation are valid. In addition, covert constraints are satisfied ($\chi = 0.05$).

Table F1 Numerical and analytical results of the covert probabilities

Node	Calculation approach of P_{covert}	$1 - P_{\text{covert}}$
Ground Willie 1	Monte Carlo based on definition (13)	0.035693
Ground Willie 1	Exact analytical expression (14)	0.035732
Ground Willie 2	Monte Carlo based on definition (13)	0.043795
Ground Willie 2	Exact analytical expression (14)	0.043741
Ground Willies	Analytical upper bound (15)	0.049981
Near UAV Willie 1	Monte Carlo based on definition (13)	0.046006
Near UAV Willie 1	Exact analytical expression (16)	0.046075
Near UAV Willie 1	Analytical approximation (17)	0.046311
Near UAV Willie 2	Monte Carlo based on definition (13)	0.045193
Near UAV Willie 2	Exact analytical expression (16)	0.045117
Near UAV Willie 2	Analytical approximation (17)	0.045806
Far UAV Willie 1	Monte Carlo based on definition (13)	0.048581
Far UAV Willie 1	Exact analytical expression (18)	0.048634
Far UAV Willie 2	Monte Carlo based on definition (13)	0.047193
Far UAV Willie 2	Exact analytical expression (18)	0.047188

Appendix G Summary of main symbols and notations

Table G1 summarizes the main symbols and notations used in this paper.

Table G1 Nomenclature of symbols and notations

Symbol/Notation	Specification
$[\mathbf{X}]_{m,n}$	The element at row m, column n of matrix $\mathbf{X}$
$\mathbf{X} \succcurlyeq 0$	Matrix $\mathbf{X}$ is positive semidefinite
$[\boldsymbol{x}]_m$	The m-th element of vector $\boldsymbol{x}$
$\|\|\boldsymbol{x}\|\|$	Euclidean norm of vector $\boldsymbol{x}$
$[x]^+$	$\max\{x, 0\}$
$\mathrm{tr}(\cdot)$, $(\cdot)^T$, $(\cdot)^*$, and $(\cdot)^H$	The trace, the transpose, the conjugate, and the conjugate transpose operators
$\mathcal{CN}(\boldsymbol{u}, \boldsymbol{\Sigma})$	Complex Gaussian distribution with mean vector $\boldsymbol{u}$ and covariance matrix $\boldsymbol{\Sigma}$
$\mathrm{U}(a, b)$	Uniform distribution from a to b
$J_\nu(\cdot)$	The ν-th order Bessel function of the first kind
$I_\nu(\cdot)$	The ν-th order modified Bessel function of the first kind
$\Pr\{\mathrm{A}\}$	The probability of event A
$\overset{\mathrm{p1}}{=}$	Equal with probability one
$\iota = \sqrt{-1}$	The imaginary unit
$\mathbf{I}_N$	$N \times N$ identity matrix
n and N	The index and the total number of symbols in one transmission
i and N_a	The index and the total number of transmit nodes
j and J_g, J_c, J_f	The index and the total number of ground Willies, near UAV Willies, far UAV Willies
$x(n)$, $v(n)$, and $n_b(n)$	Transmit symbol, interference, and the noise at Bob
$n_{g,j}(n)$, $n_{c,j}(n)$, and $n_{f,j}(n)$	The noise at the j-th ground Willie, near UAV Willie, and far UAV Willie
$\alpha(\Theta)$ and $K(\Theta)$	The path loss exponent and the Rician K-factor corresponding to elevation angle Θ
P_i and φ_i	The transmit power and the phase shift of the i-th transmit node
P_b and $P_{\max}$	The random interference power and the upper range of the interference power
ρ	Self-interference coefficient
d_b	The distance from Alice to Bob
$d_{g,i,j}$ and $d_{g,b,j}$	The distances from the i-th transmit node and Bob to the j-th ground Willie
$d_{c,i,j}$ and $d_{c,b,j}$	The distances from the i-th transmit node and Bob to the j-th near UAV Willie
$d_{f,j}$ and $d_{f,b,j}$	The distances from Alice and Bob to the j-th far UAV Willie
$d_{g,i,\min}$	The size of the protected zone of the i-th transmit node
ψ_b	The phase shift due to the propagation from the origin to Bob
$\psi_{f,j}$	The phase shift due to the propagation from the origin to the j-th far UAV Willie
$\psi_{g,b,j}$	The phase shift due to the propagation from Bob to the j-th ground Willie
$\psi_{c,b,j}$	The phase shift due to the propagation from Bob to the j-th near UAV Willie
$\psi_{f,b,j}$	The phase shift due to the propagation from Bob to the j-th far UAV Willie
W_f and w_f	Far UAV Willies' antenna gain towards Alice and that towards Bob
γ_b	The received signal-to-interference-plus-noise ratio at Bob
δ and $\delta(\boldsymbol{h}_b)$	The outage probability at Bob and that under given channel coefficients $\boldsymbol{h}_b$
P_{FA} and P_{MD}	False alarm probability and miss detection probability
ξ	The sum of P_{FA} and P_{MD}
P_{covert}	The covert probability
$\hat{P}_i$ and $\hat{P}_{\max}$	The transmit power limits of the i-th transmit node and Bob

References

1 Gradshteyn I S, Ryzhik I M. Table of integrals, series, and products, 7th ed. San Diego: Academic, 2007
2 Durgin G D, Rappaport T S, de Wolf D A. New analytical models and probability density functions for fading in wireless communications. IEEE Trans Commun, 2002, 50: 1005–1015
3 Yu Z, Chai C C, Tjhung T T. Envelope probability density functions for fading model in wireless communications. IEEE Trans Veh Technol, 2007, 56: 1907–1912
4 Sun Y, Baricz A, Zhou S D. On the monotonicity, log-concavity, and tight bounds of the generalized Marcum and Nuttall Q-Functions. IEEE Trans Inf Theory, 2010, 56: 1166–1186